The Astrophysical Journal Letters, 871:L8 (5pp), 2019 January 20 https://doi.org/10.3847/2041-8213/aafc62

Millisecond Pulsars and the Gamma-Ray Excess in Andromeda

Giacomo Fragione[1], Fabio Antonini[2,4], and Oleg Y. Gnedin[3]
[1] Racah Institute for Physics, The Hebrew University, Jerusalem 91904, Israel
[2] Faculty of Engineering and Physical Sciences, University of Surrey, Guildford, Surrey GU2 7XH, UK
[3] Department of Astronomy, University of Michigan, Ann Arbor, MI 48109, USA
Received 2018 November 29; revised 2018 December 30; accepted 2019 January 4; published 2019 January 22

Abstract

The *Fermi Gamma-Ray Space Telescope* has provided evidence for diffuse gamma-ray emission in the central parts of the Milky Way and the Andromeda galaxy. This excess has been interpreted either as dark-matter annihilation emission or as emission from thousands of millisecond pulsars (MSPs). We have recently shown that old massive globular clusters (GCs) may move toward the center of the Galaxy by dynamical friction and carry within them enough MSPs to account for the observed gamma-ray excess. In this Letter we revisit the MSP scenario for the Andromeda galaxy by modeling the formation and disruption of its GC system. We find that our model predicts gamma-ray emission ∼2–3 times larger than for the Milky Way, but still nearly an order of magnitude smaller than the observed Fermi excess in the Andromeda. Our MSP model can reproduce the observed excess only by assuming ∼8 times a larger number of old clusters than inferred from galaxy scaling relations. To explain the observations we require either that Andromeda deviates significantly from the scaling relations, or that a large part of its high-energy emission comes from additional sources.

Key words: galaxies: star clusters: general – Galaxy: center – Galaxy: kinematics and dynamics – gamma rays: diffuse background – gamma rays: galaxies – pulsars: general

1. Introduction

The gamma-ray luminosity of star-forming galaxies has been under scrutiny for a long time, as its study may provide important clues regarding the acceleration mechanisms of cosmic rays and their transport through the interstellar medium, and constrain the star formation rate as well as the gas and metallicity content of a galaxy. Thanks to the Large Area Telescope instrument on board of the *Fermi Gamma-Ray Space Telescope* (*Fermi*-LAT), new high-quality data from 20 MeV to over 300 GeV have been available to study the high-energy physics (Atwood et al. 2009). These data have revealed peculiarities of the gamma-ray emission from the inner region of our Galaxy, the so-called Fermi Bubbles —large structures extending up to 8 kpc away from the Galactic plane (Ackermann et al. 2014).

Analyses of the diffuse gamma-ray emission also found a spherically symmetric excess around the Galactic Center, peaking at ∼2 GeV and extending out to ∼3 kpc from the center (Abazajian et al. 2014; Calore et al. 2015; Lee et al. 2015; Ajello et al. 2016). Two main explanations have been proposed for the observed excess, based mainly on similarity with the radial distribution and energy spectrum of the emission. One possibility is that the excess is a product of dark-matter annihilation (Calore et al. 2015). Alternatively, the emission could be due to thousands of unresolved millisecond pulsars (MSPs; Brandt & Kocsis 2015; Bartels et al. 2016; Arca-Sedda et al. 2018; Fragione et al. 2018a, 2018b).

In addition to the Milky Way, seven external star-forming galaxies have been observed by Fermi in gamma-rays, including the Small and Large Magellanic Cloud and the Andromeda galaxy (Ackermann et al. 2012). The latter is of particular interest because it is the only other large spiral with a prominent bulge that is close enough that the disk and bulge can be resolved as separate components. Its galactic nucleus harbors a supermassive black hole and a central blue cluster (P3) surrounded by two overdensities of stars (P1 and P2), which reside on either side of P3 with a separation of ∼1.8 pc (Bender et al. 2005; Lauer et al. 2012). Ackermann et al. (2017) reported the detection of diffuse gamma-ray emission on the order $\sim 2.8 \times 10^{38}$ erg s^{-1}, which extends up to ∼5 kpc from Andromeda's center, with the significance of spatial extent at the 4σ level. Its morphology is not well constrained and can be described either by a uniform disk or a Gaussian distribution. Compared to the Milky Way's excess, the Andromeda excess is about one order of magnitude larger. Moreover, this emission does not correlate with regions rich in gas, and its spectrum is consistent with a simple power law or with a truncated power law with an exponential cutoff in the GeV range. The latter closely resembles the MSP spectral templates. As in the Galactic case, there have been claims for both the MSP and dark-matter-annihilation origin of the Andromeda's diffuse emission (McDaniel et al. 2018). Ackermann et al. (2017) suggested that, if MSPs are responsible for the emission, the ∼4–10 times higher flux in Andromeda could be attributed to the correspondingly higher number of globular clusters (GCs) in that galaxy (Barmby et al. 2001; Galleti et al. 2007). Recently, Eckner et al. (2018) proposed that the emission comes from an unresolved population of MSPs formed in situ.

In this Letter, we revisit the MSP scenario in the Andromeda galaxy. We model the formation and disruption of Andromeda GCs across all cosmic time, starting from redshift $z = 3$ to the present time, and calculate the amount of MSPs deposited in the Andromeda bulge as a consequence of cluster disruption, while accounting also for the spin-down of the MSPs due to magnetic-dipole braking.

This Letter is organized as follows. In Section 2, we describe the semi-analytical model we used to generate and evolve the primordial population of GCs. In Section 3, we show that our fiducial model underestimates the measured Andromeda

[4] STFC E. Rutherford Fellow.

excess. Finally, in Section 4, we discuss the implications of our findings and summarize our conclusions.

2. GC Evolution

In this section, we discuss the equations used to evolve the GC population; for details, see Gnedin et al. (2014). We assume that the cluster formation rate was a fraction $f_{\rm GC,i}$ of the overall star formation rate

$$\frac{dM}{dt} = f_{\rm GC,i}\frac{dM_*}{dt}. \quad (1)$$

We assume that all clusters formed at redshift $z = 3$ and calculate their subsequent evolution for 11.5 Gyr. The initial mass of the clusters is drawn from a power-law distribution

$$\frac{dN}{dM} \propto M^{-2}, \quad M_{\rm min} < M < M_{\rm max}. \quad (2)$$

We set $M_{\rm min} = 10^4\,M_\odot$ and $M_{\rm max} = 10^7\,M_\odot$.

After formation, we evolve the GC masses by taking into account mass loss via stellar winds and the removal of stars by the galactic tidal field. The mass loss is modeled assuming a Kroupa (2001) initial mass function, and adopting the main-sequence lifetime of stars from Hurley et al. (2000) and the initial–final mass relations for stellar remnants from Chernoff & Weinberg (1990). We consider mass loss due to stripping by the galactic tidal field according to

$$\frac{dM}{dt} = -\frac{M}{t_{\rm tid}} \quad (3)$$

where

$$t_{\rm tid}(r, M) \approx 10\left(\frac{M}{2\times10^5\,M_\odot}\right)^{2/3} P(r)\ {\rm Gyr} \quad (4)$$

is the typical tidal disruption time (Gieles & Baumgardt 2008), and

$$P(r) = 100\left(\frac{r}{\rm kpc}\right)\left(\frac{V_{\rm c}(r)}{\rm km\ s^{-1}}\right)^{-1} \quad (5)$$

is the (normalized) rotational period of the cluster orbit, which parametrizes the strength of the local galactic field, and $V_{\rm c}(r)$ is the circular velocity at a distance r from the Galactic Center.

We assume that the cluster is torn apart when the stellar density at a characteristic radius, such as the half-mass–radius, falls below the mean local galactic density

$$\rho_{\rm h} < \rho_*(r) = \frac{V_{\rm c}^2(r)}{2\pi G r^2}, \quad (6)$$

due to the adopted field stellar mass, as well as the growing mass of the nuclear star cluster (NSC). Following Gnedin et al. (2014), we adopt the average density at the half-mass–radius

$$\rho_h = \begin{cases} 10^3\,M_\odot\ {\rm pc}^{-3} & \text{for } M \leqslant 10^5\,M_\odot \\ 10^3\left(\frac{M}{10^5\,M_\odot}\right)^2 M_\odot\ {\rm pc}^{-3} & \text{for } 10^5\,M_\odot < M < 10^6\,M_\odot \\ 10^5\,M_\odot\ {\rm pc}^{-3} & \text{for } M \geqslant 10^6\,M_\odot \end{cases} \quad (7)$$

The cluster mass M here is the current value before disruption, not the initial mass. As the NSC builds up in mass, its stellar density eventually begins to exceed the densities within the infalling GCs, which will be directly disrupted before reaching the center of the galaxy (e.g., Antonini 2013).

As in Gnedin et al. (2014), we assume the clusters to orbit on a circular trajectory of radius r and take this radius to be the time-averaged radius of the true, likely eccentric, cluster orbit. We consider the effect of dynamical friction on cluster orbits by evolving the orbital radius r

$$\frac{dr}{dt} = -\frac{r^2}{t_{\rm df}}, \quad (8)$$

where

$$t_{\rm df}(r, M) \approx 0.45\left(\frac{M}{10^5\,M_\odot}\right)^{-1}\left(\frac{r}{\rm kpc}\right)^2\left(\frac{V_{\rm c}(r)}{\rm km\ s^{-1}}\right){\rm Gyr}. \quad (9)$$

We also include a correction for the non-zero eccentricities of the cluster orbits, $f_e = 0.5$ (for details see Jiang et al. 2008; Gnedin et al. 2014).

2.1. Andromeda Potential Model

We describe the Andromeda gravitational potential with a three-component model $\Phi = \Phi_b + \Phi_{\rm disk} + \Phi_{\rm halo}$, where

1. Φ_b is the contribution of a spherical bulge,
$$\Phi_b(r) = -\frac{GM_b}{r + a_b}, \quad (10)$$
with mass $M_b = 1.9\times10^{10}\,M_\odot$ and core radius $a_b = 1$ kpc;
2. Φ_d is the contribution of an axisymmetric disk,
$$\Phi_d(R, z) = -\frac{GM_d}{\sqrt{(R^2 + (b + \sqrt{c^2 + z^2})^2)}}, \quad (11)$$
with mass $M_d = 8\times10^{10}\,M_\odot$, length scale $b = 5$ kpc and scale height $c = 1$ kpc;
3. $\Phi_{\rm halo}$ is the contribution of a spherical dark-matter halo
$$\Phi_{\rm DM}(r) = -\frac{GM_{\rm DM}\ln(1 + r/r_s)}{r}. \quad (12)$$
with $M_{\rm DM} = 2\times10^{12}\,M_\odot$ and length scale $r_s = 35$ kpc.

The adopted parameters match the observed maximum circular velocity (van der Marel et al. 2014; Patel et al. 2017).

3. Gamma-Ray Excess in Andromeda

In our model, everything has been fixed apart from the initial amount of galactic mass locked in GCs. The initial cluster mass fraction $f_{\rm GC,i}$ is generally of the order of a few percent, but its exact value is difficult to estimate. In the case of the Milky Way, it can be fixed by assuming that a certain fraction of the NSC was accreted by inspiraling GCs (Fragione et al. 2018a). To overcome this problem, we make use of a strong correlation between the present-day mass of the GC population and the host halo that emerges both from observations and models (e.g., Harris et al. 2017; Choksi et al. 2018)

$$M_{\rm GC} = 3.4\times10^{-5}\,M_{\rm DM}. \quad (13)$$

with an intrinsic scatter of $\sigma = 0.2$ dex. Thus we set $f_{\rm GC,i} = 0.0075$, which gives a final present-day mass of the

GC system in Andromeda that agrees within 1σ with Equation (13).

We evolve the GC population according to the model in Section 2 and compute the mass deposited by each cluster as a function of time t and radius r from Andromeda's galactic center. Then we calculate the total amount of gamma-ray luminosity expected from all MSPs left in the cluster debris, by using the mean relation between the gamma-ray emission from GCs and their masses (Fragione et al. 2018a)

$$\log \frac{L_\gamma}{M_{\rm GC}} = 32.66 \pm 0.06 - (0.63 \pm 0.11) \log M_{\rm GC}, \quad (14)$$

where L_γ is the gamma-ray emission of a GC in erg s^{-1}, and $M_{\rm GC}$ is its mass in units of $M_\odot$. Alternatively, we also consider models with

$$\frac{L_\gamma}{M_{\rm GC}} = {\rm const} = 4.57 \times 10^{29}\,{\rm erg\,s^{-1}} M_\odot^{-1}, \quad (15)$$

to test the dependence of our results on the adopted L_γ–$M_{\rm GC}$ relation. We then generate individual MSPs by sampling from a power-law distribution

$$\frac{dN}{dL_\gamma} \propto L_\gamma^{-\alpha}, \quad (16)$$

with $\alpha = 1$, between $L_{\gamma,\rm min} = 10^{31}$ erg s^{-1} and $L_{\gamma,\rm max} = 10^{36}$ erg s^{-1} (Ajello et al. 2016). We sample from the above distribution until the total luminosity from the deposited MSPs equals $L_{\gamma,\rm tot}^{\rm dep}(t)$. This gives us the number of MSPs, $N_{\rm MSP}(t)$.

From the moment that MSPs are deposited in the galactic center, we evolve in time the gamma-ray luminosity of a given pulsar as

$$L_\gamma(t) = \frac{L_{\gamma,0}}{[1 + (t/\tau)^{1/2}]^2}, \quad (17)$$

where $L_{\gamma,0}$ is the initial luminosity and τ is the characteristic spin-down timescale for a MSP to lose its rotational kinetic energy due dipole magnetic breaking

$$\tau = \frac{E}{\dot{E}} = \frac{P}{2\dot{P}}, \quad (18)$$

where P and $\dot{P}$ are the MSP rotational period and its derivative, respectively. As discussed in Fragione et al. (2018a), we adopt two models for the MSP spin-down. The first model (Model LON) uses observations of the MSP population in 47 Tuc, and τ is given by (Prager et al. 2017)

$$\tau = \frac{c}{1.59 \times 10^{-9}\,{\rm m\,s^{-2}}} \left(\frac{2 \times 10^8\,{\rm G}}{B}\right)^2 \left(\frac{P}{2\,{\rm ms}}\right)^2, \quad (19)$$

where c is the speed of light and B is the magnetic field. In this model, the τ distribution has a mean around 1 Gyr, but also a non-negligible tail at larger τ's. In the second model (Model GAU), we adopt a Gaussian distribution with mean of 3 Gyr, consistent with Freire et al. (2001), who found a characteristic age of ≈3 Gyr for MSPs in NGC 104. We note that recently O'Leary et al. (2016) claimed that $L_\gamma \propto (1 + (t/\tau)^{1/2})^{-1}$ is more consistent with the data, which would give a less important spin-down of MSP luminosities. The shape of the τ distribution and its relation to L_γ turn out to be the two most important ingredients controlling the final contribution of the excess, but both of them are still quite uncertain (Fragione et al. 2018a). Table 1 summarizes the models considered in the present work.

In Figure 1, we illustrate the predicted MSP integrated gamma-ray luminosity at 2 GeV within a distance r from Andromeda's center. We found that the total gamma-ray luminosity is $\sim 1.6 \times 10^{37}$ erg s^{-1} and $\sim 3.5 \times 10^{37}$ erg s^{-1} for Model GAU-EQ and Model LON-EQ, respectively. As already noted in Fragione et al. (2018a), we found that the models that use the Prager et al. (2017) prescription for the spin-down rate predict a flux about two times larger than the models with the Freire et al. (2001) τ distribution. We also ran models with a constant value of gamma-ray luminosity to mass ratio to compute the total amount of gamma-ray flux in cluster debris. In these latter models, the overall flux at $r \lesssim 1$ kpc is increased by about an order of magnitude, but the total luminosity is comparable.

3.1. Model Uncertainties

In our fiducial model LON-C, the MSP scenario does not reproduce the observed gamma-ray flux measured at the center of Andromeda. Yet, there are some important uncertainties in our approach, apart from the MSP spin-down model (see also discussion in Fragione et al. 2018a).

An important factor that can affect the results is the initial cluster mass fraction. In the models described above, we fixed $f_{{\rm GC},i}$ by requiring that the present-day mass of the GC system agrees with the cosmological scaling relation (Equation (13)). To check the effect of this parameter, we ran Model FGCI, where we consider $0.0075 \leqslant f_{{\rm GC},i} \leqslant 0.06$. The other parameters are set as in the fiducial Model LON-C. Figure 2 shows the resulting MSP integrated gamma-ray luminosity within a distance r from Andromeda's center as a function of the initial amount of mass in GCs. Our MSP model can reproduce the observed *Fermi* excess only for $f_{{\rm GC},i} \approx 0.06$; this is ∼8 larger than the $f_{{\rm GC},i}$ inferred from Equation (13) and predicts a larger number of clusters in Andromeda than expected (Barmby et al. 2001).

In our main model, we fixed $M_{\rm min} = 10^4\,M_\odot$ and $M_{\rm max} = 10^7\,M_\odot$. Our results are essentially independent on $M_{\rm min}$, because low-mass clusters dissolve quickly (Gnedin et al. 2014). We explore the effect of varying $M_{\rm max}$ on our results (Model MMAX; see Table 1). We find that a larger $M_{\rm max}$ implies a larger gamma-ray excess, but only by a small factor. More specifically, we find that the integrated MSP gamma-ray luminosity is $\sim 2.9 \times 10^{37}$ erg s^{-1} and $\sim 3.6 \times 10^{37}$ erg s^{-1} for $M_{\rm max} = 5 \times 10^6\,M_\odot$ and $M_{\rm max} = 3 \times 10^7\,M_\odot$, respectively. These results demonstrate that the integrated gamma-ray luminosity predicted by our models is only marginally affected by the choice of $M_{\rm max}$.

Another source of uncertainty is the parametrization of the typical timescales for cluster evolution and ρ_h. In the case of Equation (7), we take the lower limit from the typical observed density of low-mass Galactic GCs. More massive clusters are expected to be in the expansion phase to fill their Roche lobes, during which $\rho_h \propto M^2$ (Gieles et al. 2011). The upper limit for the most massive clusters ($\rho_{\rm h} = 10^5\,M_\odot\,{\rm pc}^{-3}$) corresponds roughly to the highest observed half-mass density of Galactic GCs. For what concerns Equation (5), we have revised the normalization of $P(r)$, hence of Equation (4), relative to our first paper (Fragione et al. 2018a) by a factor of ∼2.5, to account for the longer disruption time in detailed N-body

Table 1

Model, Spin-down (τ), Initial Cluster Mass Fraction ($f_{GC,i}$), Maximum GC Mass (M_{max}), Gamma-Ray Luminosity-to-mass Ratio (L_γ/M_{GC}), Maximum Luminosity of MSPs ($L_{\gamma,max}$), Slope of the MSP Luminosity Distribution (α), Mass of Andromeda Bulge (M_b), Total Gamma-Ray Luminosity at 5 kpc (L_γ^5)

Model	$f_{GC,i}$	M_{max} ($M_\odot$)	L_γ/M_{GC}	τ (Gyr)	$L_{\gamma,max}$ (erg s^{-1})	α	M_b ($M_\odot$)	$L_{\gamma,5}$ (erg s^{-1})
LON-EQ	0.0075	10^7	Equation (14)	Prager+2017	10^{36}	1	1.9×10^{10}	3.3×10^{37}
LON-C	0.0075	10^7	const	Prager+2017	10^{36}	1	1.9×10^{10}	3.3×10^{37}
GAU-EQ	0.0075	10^7	Equation (14)	Freire+2001	10^{36}	1	1.9×10^{10}	1.4×10^{37}
GAU-C	0.0075	10^7	const	Freire+2001	10^{36}	1	1.9×10^{10}	1.4×10^{37}
FGCI	0.0075-0.06	10^7	const	Prager+2017	10^{36}	1	1.9×10^{10}	3.3–21×10^{37}
MMAX	0.0075	0.5–3×10^7	const	Prager+2017	10^{36}	1	1.9×10^{10}	2.9–3.6×10^{37}
LMAX	0.0075	10^7	const	Prager+2017	10^{35}–10^{36}	1	1.9×10^{10}	2.9–3.3×10^{37}
ALPHA	0.0075	10^7	const	Prager+2017	10^{36}	0.5–1.5	1.9×10^{10}	3.1–3.5×10^{37}
MBUL	0.0075	10^7	const	Prager+2017	10^{36}	1	0.5–4×10^{10}	1.9–3.6×10^{37}

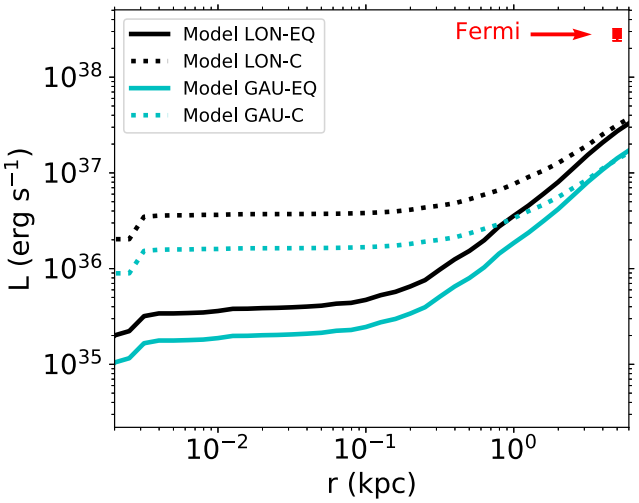

Figure 1. Predicted MSP integrated gamma-ray luminosity within a distance r from Andromeda's center. The red data point represents the luminosity as measured by *Fermi*.

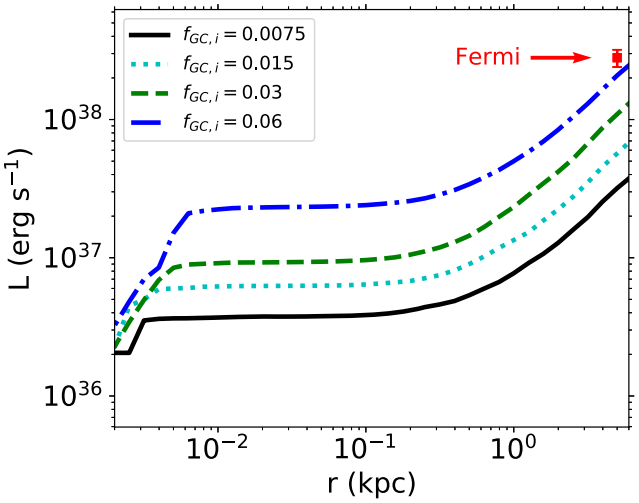

Figure 2. Predicted MSP integrated gamma-ray luminosity within a distance r from Andromeda's center as function of the initial amount of mass in GCs (Model FGCI). The red data point represents the luminosity as measured by *Fermi*.

simulations of Lamers et al. (2010). However, by comparing our current models to the ones presented in Fragione et al. (2018a), we found no significant effect on the results.

Finally, we do not consider eccentric GC orbits in our model; rather, we include the effect of the deviation of the cluster's orbit from circular by taking into account a correction factor $f_e = 0.5$ in Equation (8), which is consistent with the results of simulations by Jiang et al. (2008). We note that eccentric orbits may have shorter dynamical friction timescales, increase the mass-loss rate, and shorten the GC relaxation time. Thus, some of the clusters may get disrupted earlier than clusters on circular orbits. Unfortunately, the primordial distribution of cluster eccentricities is not known, which makes it difficult to quantify its effect. However, we note that the simple prescriptions for dynamical friction as implemented here reproduce well the spatial and mass distribution of GCs in our Galaxy (Gnedin et al. 2014).

Also the parameters defining the MSP luminosity distribution can play a role. In our fiducial model (Model LON-C), we set the slope of the distribution $\alpha = 1$, and $L_{\gamma,min} = 10^{31}$ erg s^{-1} and $L_{\gamma,max} = 10^{36}$ erg s^{-1}. While $L_{\gamma,min}$ does not play a significant role (Fragione et al. 2018a), we investigate the impact of $L_{\gamma,max}$ and α on our results (see Table 1). We repeated our calculations with $L_{\gamma,max}$ reduced to 10^{35} erg s^{-1} (Model LMAX), and found that the total gamma-ray excess is reduced by $\sim$10% with respect to our fiducial model. Also, we considered α in the range 0.5–1.5 (Model ALPHA). Smaller α's (shallower distributions) imply a larger gamma-ray emission, while larger α's (steeper distributions) lead to a smaller total excess. In any case, the Andromeda excess results $\sim$5% bigger and $\sim$5% smaller for $\alpha = 0.5$ and $\alpha = 1.5$, respectively, than our fiducial model.

We also check the effect of varying the parameters defining the Andromeda bulge mass M_b, which may be an important parameter for the GC survivability in the galaxy innermost regions. We find that the integrated gamma-ray excess is $\sim 1.9 \times 10^{37}$ erg s^{-1} and $\sim 3.6 \times 10^{37}$ erg s^{-1} when $M_b = 0.5 \times 10^{10}$ and $M_b = 4 \times 10^{10}$, respectively, and still smaller than the observed one. Finally, we also ran models adopting different values of the Andromeda bulge scale radius a_b, but we did not find any significant difference in the total gamma-ray flux compared to our fiducial Model LON-C.

Table 1 reports all of the models we investigated and their total gamma-ray luminosity within 5 kpc ($L_{\gamma,5}$).

4. Conclusions

The *Fermi* Telescope has revealed a gamma-ray excess around our Galactic Center (out to $\sim$3 kpc) of the order of $\sim 10^{37}$ erg s^{-1}, which has been interpreted either as dark-matter-annihilation emission or as emission of thousands of

MSPs. *Fermi* also showed evidence of a diffuse gamma-ray emission ($\sim 2.8 \times 10^{38}$ erg s^{-1}) also in the center (up to $\sim$5 kpc) of the Andromeda galaxy. As in the case of the Galactic Center, there have been suggestions for both a MSP and for a dark-matter-annihilation emission.

In this Letter, we have revisited the MSP scenario in the Andromeda galaxy, by modeling the formation and disruption of GCs that can deliver thousands of MSPs in the bulge. We have modeled the MSP gamma-ray emission by taking into account also the spin-down due to magnetic-dipole braking, and found that the total gamma-ray luminosity is $\sim$1.6-3.5 $\times$ 10^{37}, i.e., nearly one order of magnitude smaller than the observed excess. Our MSP model can reproduce the *Fermi* excess only by assuming a number of primordial clusters that is $\sim$8 times larger than that inferred from the galactic scaling relations.

Recently, Eckner et al. (2018) proposed that the emission from an unresolved population of MSPs formed in situ can account for $\sim 7 \times 10^{37}$ erg s^{-1} of the excess. While both our model and the Eckner et al. (2018) model cannot account for all the observed excess, they can explain nearly half of it when taken together. We also note that M31 likely had a burst of star formation $\sim$1–2 Gyr ago, which could boost both the abundance of close binaries and massive star clusters up to a factor of $\sim$2 (Dong et al. 2018). A combination of all these factors could provide the astrophysical origin of the gamma-ray emission in the Andromeda galaxy.

Finally, we note that some of the neutron stars delivered by the GCs may mass-segregate to some extent and also be successfully exchanged in few-body interactions in binaries that later could lead to the formation of MSPs, which could enhance our predicted rate (Leigh et al. 2016). This would give a maximum contribution roughly comparable to the in situ formation scenario, which can account only for $\sim 1/4$ of the excess (Eckner et al. 2018), being the mass in GCs of the order of the mass of the nuclear star cluster. However, the details of binary modeling would be the same for Andromeda and our Galaxy, while the observed gamma-ray fluxes are very different. Hence, MSPs delivered by GCs cannot explain both the Milky Way and Andromeda fluxes, and therefore other sources of gamma-rays in M31 center are required.

G.F. is supported by the Foreign Postdoctoral Fellowship Program of the Israel Academy of Sciences and Humanities. G.F. also acknowledges support from an Arskin postdoctoral fellowship at the Hebrew University of Jerusalem. F.A. acknowledges support from an E. Rutherford fellowship (ST/P00492X/1) from the Science and Technology Facilities Council. O.G. was supported in part by the NSF through grant 1412144.

ORCID iDs

Giacomo Fragione https://orcid.org/0000-0002-7330-027X
Fabio Antonini https://orcid.org/0000-0003-3138-6199
Oleg Y. Gnedin https://orcid.org/0000-0001-9852-9954

References

Abazajian, K. N., Canac, N., Horiuchi, S., & Kaplinghat, M. 2014, PhRvD, 90, 023526
Ackermann, M., Ajello, M., Allafort, A., et al. 2012, ApJ, 755, 164
Ackermann, M., Ajello, M., Albert, A., et al. 2017, ApJ, 836, 208
Ackermann, M., Albert, A., Atwood, W. B., et al. 2014, ApJ, 793, 64
Ajello, M., Albert, A., Atwood, W. B., et al. 2016, ApJ, 819, 44
Antonini, F. 2013, ApJ, 763, 62
Arca-Sedda, M., Kocsis, B., & Brandt, T. 2018, MNRAS, 479, 900
Atwood, W. B., Abdo, A. A., Ackermann, M., et al. 2009, ApJ, 697, 1071
Barmby, P., Huchra, J. P., & Brodie, J. P. 2001, AJ, 121, 1482
Bartels, R., Krishnamurthy, S., & Weniger, C. 2016, PhRvL, 116, 051102
Bender, R., Kormendy, J., Bower, G., et al. 2005, ApJ, 631, 280
Brandt, T. D., & Kocsis, B. 2015, ApJ, 812, 15
Calore, F., Cholis, I., McCabe, C., & Weniger, C. 2015, PhRvD, 91, 063003
Chernoff, D. F., & Weinberg, M. D. 1990, ApJ, 351, 121
Choksi, N., Gnedin, O. Y., & Li, H. 2018, MNRAS, 480, 2343
Dong, H., Olsen, K., Lauer, T., et al. 2018, MNRAS, 478, 5379
Eckner, C., Hou, X., Serpico, P. D., et al. 2018, ApJ, 862, 79
Fragione, G., Antonini, F., & Gnedin, O. Y. 2018a, MNRAS, 475, 5313
Fragione, G., Pavlík, V., & Banerjee, S. 2018b, MNRAS, 480, 4955
Freire, P. C., Kramer, M., Lyne, A. G., et al. 2001, ApJL, 557, L105
Galleti, S., Bellazzini, M., Federici, L., Buzzoni, A., & Fusi Pecci, F. 2007, A&A, 471, 127
Gieles, M., & Baumgardt, H. 2008, MNRAS, 389, L28
Gieles, M., Heggie, D. C., & Zhao, H. 2011, MNRAS, 413, 2509
Gnedin, O. Y., Ostriker, J. P., & Tremaine, S. 2014, ApJ, 785, 71
Harris, W. E., Blakeslee, J. P., & Harris, G. L. H. 2017, ApJ, 836, 67
Hurley, J. R., Pols, O. R., & Tout, C. A. 2000, MNRAS, 315, 543
Jiang, C. Y., Jing, Y. P., Faltenbacher, A., Lin, W. P., & Li, C. 2008, ApJ, 675, 1095
Kroupa, P. 2001, MNRAS, 322, 231
Lamers, H. J. G. L. M., Baumgardt, H., & Gieles, M. 2010, MNRAS, 409, 305
Lauer, T. R., Bender, R., Kormendy, J., Rosenfield, P., & Green, R. F. 2012, ApJ, 745, 121
Lee, S. K., Lisanti, M., & Safdi, B. R. 2015, JCAP, 5, 56
Leigh, N. W. C., Antonini, F., Stone, N. C., Shara, M. M., & Merritt, D. 2016, MNRAS, 463, 1605
McDaniel, A., Jeltema, T., & Profumo, S. 2018, PhRD, 97, 103021
O'Leary, R. M., Meiron, Y., & Kocsis, B. 2016, ApJL, 824, L12
Patel, E., Besla, G., & Sohn, S. T. 2017, MNRAS, 464, 3825
Prager, B. J., Ransom, S. M., Freire, P. C., et al. 2017, ApJ, 845, 148
van der Marel, R. P., Fardal, M., Besla, G., et al. 2014, ApJ, 753, 8